Electrode Position Optimization in Electrical Impedance Tomography

Joshua Zhang

December 1 2025

1 Introduction

Electrical impedance tomography (EIT) is a non-invasive imaging technique that aims to reconstruct a conductivity distribution inside an object using boundary data measurements. The applications of EIT span many different fields–for example, biomedical imaging and strain analysis in civil engineering. In practice, a discrete set of electrodes is placed on the boundary of the object, where current is injected and potentials are measured; this is referred to as the complete electrode model (CEM). There are two main problems in EIT: i) the forward problem and ii) the inverse problem. The forward problem aims to predict boundary voltage measurements when internal conductivity and other boundary data (current injections, electrode contact impedances) are provided, while the inverse problem aims to reconstruct the conductivity distribution given measured voltages and currents injected at the electrodes [1].

Solving problems in EIT present many challenges–notably, the diffusive nature of electric fields provides a low spatial resolution, and ill-posedness of the inverse problem leads to sensitivity of conductivity to boundary measurements. Thus, electrode location optimization is motivated by the goal of maximizing the quality of information in EIT measurements and improving conditioning of the inverse problem, thereby improving the robustness and quality of inverse solves in practice. However, previous works to address this problem employ optimizations that are either computationally demanding or depend on prior knowledge of the conductivity distribution [2]. On the other hand, advancements in deep-learning has flourished novel methods for EIT image reconstruction, with CNNs and GNNs being among popular architectures [3]. In this project, we will describe a deep learning-based algorithm from [4] which computes optimal electrode placements for 2-dimensional EIT problems and seeks to maximize the measurement quality of voltages. This approach addresses the deficiencies in previous works as the algorithm is both fast and memory-efficient while at the same time does not require prior knowledge on the target conductivity distribution, and is shown to outperform "standard" electrode configurations in metrics related to discretization errors, conditioning, inverse reconstructions, and distinguishability.

2 Background

This section will outline the forward and inverse problem setups under the complete electrode model, as well as justify the setup of the algorithm's neural network parameters.

2.1 Complete Electrode Model

Consider a domain $\Omega \subset \mathbb{R}^2$ and k electrodes $\{e_j\}_{j=1}^k$ (electrodes can have lengths, i.e. not points) along $\partial\Omega$ with currents $I = (i_1, ..., i_k)$ injected at each electrode, and potentials $V = (v_1, ..., v_k)$ are measured at each electrode. Note that these potentials can only be measured with respect to another source (e.g. a ground or another electrode); in the case of measuring boundary voltages on electrode pairs, we need to specify a measurement pattern $M \in [k]^{2\times m}$, where m is the number of measurements and $[k] = \{1, 2, ...k\}$. It is necessary that $\sum_{j=1}^k i_j = 0$ and $\sum_{j=1}^k u_j = 0$. Each electrode also has a contact impedance $z_k > 0$. Furthermore, the domain is discretized into a grid, so that the continuous σ can be interpolated at a finite set of points; this paper uses the EIDORS unstructured meshing [5].

Thus, the forward problem aims to find a potential map U such that

$$V = U(\{\Omega, \sigma, \{e_j\}, \{z_j\}, I\}) \tag{1}$$

and the inverse problem aims to recover σ given $\{I, V\}$. An example of a technique to solve this is to minimize σ over a least square fit:

$$\|V_s - U(\{\Omega, \sigma, \{e_j\}, \{z_j\}, I\})\|^2 \tag{2}$$

where V_s are a set of measured voltages on the boundary. Note that this requires a forward solve of U at every iteration. Furthermore, CEM simplifies the setup to a boundary value problem and also requires the following to hold:

$$\Delta u = 0 \qquad x \in \Omega \setminus \partial\Omega \tag{3}$$

$$\sigma \partial_n u = 0 \qquad x \in \partial\Omega \setminus \{e_j\} \tag{4}$$

$$u + z_j \sigma \partial_n u = v_j \qquad x \in \{e_j\} \tag{5}$$

$$\int_{e_j} \sigma \partial_n u \mathrm{d}l = i_j \qquad j \in [k] \tag{6}$$

$$\sum_{j=1}^{k} i_j = 0 \qquad \sum_{j=1}^{k} u_j = 0 \tag{7}$$

$$u^+ - u^- = 0 \qquad x \in \partial\Omega \tag{8}$$

$$\sigma \partial_n u^+ - \sigma \partial_n u^- = 0 \qquad x \in \partial\Omega \tag{9}$$

where u^+, u^- denote the values of u on two sides of the boundary, implying continuity [1].

2.2 Parameters for Conditioning and Ill-Posedness

Let us rewrite (1) as $V = U(\sigma)$ for simplicity. It is evident that U is highly nonlinear in σ, and thus solving the inverse problem depends highly on U. Unfortunately, the inverse problem is highly ill-posed [1] (small fluctuations in U result in large fluctuations in σ), implying that the sensitivity matrix $J = \frac{\partial U(\sigma)}{\partial \sigma}$ will be highly ill-conditioned. We can also study the ill-conditioning of the hessian approximation, $H = J^T J$, which correlates directly to the ill-posedness of least square solutions of the inverse problem [6]. Thus, a good parameter to analyze for reducing conductivity sensitivity to data is the condition number:

$$\kappa(H) = \|H\|_2 \|H^{-1}\|_2 \tag{10}$$

The next parameter to analyze is derived from considering the inverse EIT problem in the context of a Gauss-Newton algorithm. Consider a set of measurements V_t; we want to find the minimizing σ such that $U(\sigma)$ is closest to V_t in least squares sense. In practice, we also need a method to generate σ samples for training. The method outlined in this paper is to use a blob-line structure–first, define a covariance matrix $\Gamma \in \mathbb{R}^{N \times N}$, with N being number of mesh points, and

$$\Gamma(i,j) := a e^{-\frac{\|x_i - x_j\|}{2b}} + c\delta_{ij} \tag{11}$$

where $a, b, c > 0$, δ_{ij} is the Kronecker delta, and x_i, x_j are mesh points. Then, define the inverse Cholesky factorization $L^T L = \Gamma^{-1}$ and a random vector $r \in \mathbb{R}_+^N$ to generate $\sigma_{rand} = L^{-1} r$. Note that since the EIDORS meshing routine is unstructured, linear interpolation of Γ onto a different-sized mesh may be necessary in training. Additionally, sufficiently large (more than 500) sample sizes minimizes the effect of any structure on σ_{rand} resulting from the coefficients a, b, c.

Now suppose that we have an initial distribution σ_0, which is taken to be the mean of a sample σ_{rand} generated from Γ. Then a one step Gauss-Newton estimate gives us:

$$\hat{\sigma} = \sigma_0 + (H(\sigma) + \Gamma^{-1})^{-1} J(\sigma_0)^T (V_t - U(\sigma_0)) \tag{12}$$

We can interpret $\hat{\sigma}$ as an approximate reconstruction of the optimum. Thus, a good parameter to measure reconstruction quality is the squared error:

$$\beta = \|\sigma_{rand} - \hat{\sigma}\|^2 \tag{13}$$

To conclude this section, we have derived $\kappa(H)$ and β as two scalar-valued parameters that capture essential information to address EIT challenges–the former focuses on data sensitivity and conditioning, and the latter on reconstruction quality. These will make up the memory-efficient input $\Theta = [\kappa, \beta]^T$ for the neural network described in the following section. Note that the theoretically optimal Θ for an EIT setup would be $[1, 0]^T$.

3 Deep Learning Algorithm

In the context of deep learning, we broadly aim to learn a mapping $Q : X \to Y$, where X, Y are input and output parameter spaces. In our case, we want our output to be the space of k electrode positions. For each electrode on the boundary, the model will consider its location purely in terms of its midpoint $[x_j, yj]^T$. Thus, each electrode configuration is a vector in $\mathbb{R}^{2k}$, and our neural network is the map

$$E = Q_{\bar{\Theta}\bar{E}}(\Theta) \tag{14}$$

where $\Theta = [\kappa, \beta]^T$ are the input parameters for an electrode configuration, E is the location vector of the k electrodes, and $\bar{\Theta}, \bar{E}$ are the dataset's input and outputs. For a dataset composed of $N_{\bar{E}}$ electrode configurations and N_σ sampled conductivities, $\bar{\Theta} \in \mathbb{R}^{2\times N_{\bar{E}} N_\sigma}$, and $\bar{E} \in \mathbb{R}^{2k\times N_{\bar{E}} N_\sigma}$, with each column of the matrices corresponding to the input/output for one datum.

Through a preliminary error analysis involving different neural network architectures and training data, assumptions on several variables for per-model training are found to be necessary to ensure effectiveness of the trained mapping and prevent over-parameterization. Thus, the training of $Q_{\bar{\Theta}\bar{E}}$ is limited to experiments with i) fixed geometry Ω, ii) fixed k number of electrodes, iii) fixed number of electrodes per side of Ω, iv) fixed forward method, v) fixed impedances $\{z_j\}$, vi) fixed injection I and measurement patterns M, and vii) fixed maximum mesh element size δ_e.

The neural network architecture consists of two hidden layers, with number of neurons computed from the method described in [7]. To train $Q_{\bar{\Theta}\bar{E}}$, backpropagation with conjugate gradient and Fletcher-Reeves updates is employed, as described in [8]. The loss function is taken as a standard sum-of-squares:

$$\mathcal{L} = \frac{1}{N_{\bar{E}} N_\sigma} \sum_{i=1}^{N_{\bar{E}} N_\sigma} (E_i - E_i^Q)^2 + \alpha \|w\|^2 \tag{15}$$

where E_i are the electron positions for sample i, E_i^Q are the network's predicted positions for sample i. α was set to be 0.01 here for the ℓ^2 regularization term to avoid overfitting, and the halting condition is $\mathcal{L} < 10^{-7}$. The prediction on testing set uses the optimal parameters as input–$Q_{\bar{\Theta}\bar{E}}([1, 0]^T)$. A schematic of the architecture can be seen in Figure 1. The authors of [4] note that training this model using 8 cores and 32GB RAM with parallel computations in MATLAB took less than 5 minutes.

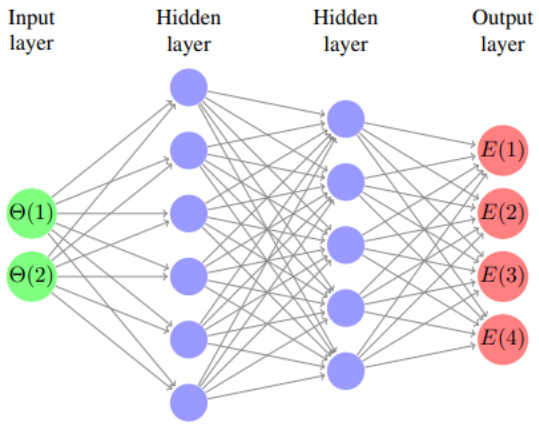

Figure 1: Two-layer neural network architecture maps parameters to output positions of 2 electrodes, $E = [x_1, x_2, y_1, y_2]^T$

A summary of the entire pipeline in pseudocode is also presented in Algorithm 1.

Algorithm 1 Data Generation and Network Training for Optimization of Electrode Positions

Initialize Ω, *elwidth*, k, δ_e, $N_{\bar{E}}$, N_σ, I, M, z, α
% Generate training data $\bar{E}$ and $\bar{\Theta}$
for $i = 1 : N_{\bar{E}}$ **do**
  $E^e = [\bar{x}_i; \bar{y}_i]$ % Init. random electrode positions
  $\Omega^e = f(E^e, \Omega, \delta_e, elwidth)$ % Generate mesh
  $\Gamma = \Gamma(\Omega^e)$ % Construct covariance matrix
  if $i = 1$ **then**
    for $\ell = 1{:}N_\sigma$ **do**
      $\bar{\sigma}_{\text{rand},\ell} = L^{-1}r$ % Make N_σ conductivities
    end for
  end if
  for $j = 1 : N_\sigma$ **do**
    if $j > 1$ **then**
      % Interpolate sample to current mesh
      $\bar{\sigma}_{\text{rand},j} \to \sigma_{\text{rand},j}$
    end if
    % Forward solve for measurements
    $V_t = U(\sigma_{\text{rand},j}, \Omega^e, I, M, z)$
    $J = \dfrac{\partial U}{\partial \sigma_{\text{rand},j}}$ % Sensitivity matrix
    $H = J^T J$ % Hessian approx
    $\kappa = \|H^{-1}\|\|H\|$ % Condition number
    $\sigma_0 = \text{mean}(\sigma_{\text{rand},j})$ % Mean as initial guess
    $J(\sigma_0) = \dfrac{\partial U}{\partial \sigma}(\sigma_0)$ % Sensitivity matrix at σ_0
    $H(\sigma_0) = J(\sigma_0)^T J(\sigma_0)$ % Hessian at σ_0
    % Gauss-Newton update
    $\Delta\sigma = (H(\sigma_0) + \Gamma^{-1})^{-1} J(\sigma_0)^T (V_t - U(\sigma_0))$
    $\hat{\sigma} = \sigma_0 + \Delta\sigma$
    $\beta = \|\hat{\sigma} - \sigma_{rand,j}\|^2$ % Conductivity misfit
    $\theta(:, j) = [\kappa,\ \beta]^T$ % Collect input params
    $\varepsilon(:, j) = E^e$ % Collect output params
  end for
  $\bar{\Theta} = [\bar{\Theta}, \theta]$, $\bar{E} = [\bar{E}, \varepsilon]$
end for
% Network training
% # neurons for layer 1
$L_1 = \lfloor ((k+2)N_{\bar{E}})^{1/2} + 2 \times (N_E/(k+2))^{1/2} \rfloor$
% # neurons for layer 2
$L_2 = \lfloor k \times (N_{\bar{E}}/(k+2))^{1/2} \rfloor$
% CG backprop w/ Fletcher–Reeves Training
$Q_{\bar{\Theta},\bar{E}} = \texttt{train}(\bar{\Theta}, \bar{E}, L_1, L_2, \alpha)$
% Compute optimized electrode positions
$E = Q_{\bar{\Theta},\bar{E}}([1, 0]^T)$
`return` E

4 Experiments

To quantify the results of our algorithm, we first identify metrics relating to the reliability, conditioning, conductivity reconstructability, and distinguishability of the optimized electrode locations.

4.1 Metrics

First, to address reliability, we consider discretization errors–indeed, an electrode configuration E is reliable if voltages computed on coarse and fine meshes are similar (ideally identical) for any internal conductivity σ. We define the mean error:

$$\mu_E = \frac{1}{N_b} \sum_{j=1}^{N_b} (U_A(\sigma_j) - U_r(\sigma_j)) \tag{16}$$

over N_b test conductivity samples, between U_A, a forward model on a fine mesh, and U_r a reduced model on a coarser mesh. By sampling many voltage predictions on the boundary, μ_E becomes a vector so we consider the norm $\|\mu_E\|_1$ as a metric (to minimize).

Next, to address conditioning and the ill-posedness of the Hessian approximation [6], we can examine the average condition number:

$$\bar{\kappa}_E = \frac{1}{N_b} \sum_{j=1}^{N_b} \kappa(H(\sigma_j)) \tag{17}$$

averaged over N_b conductivity samples. This metric correlates with sensitivity of reconstructions to boundary data, which we seek to minimize.

Additionally, we have a metric for inverse reconstruction quality, determined by sensitivity to noisy voltage measurements. Inverse reconstructions for this experiment use a least-squares approach by considering the cost function:

$$\Psi(\sigma) = \|L_n(V_s - U(\sigma)\|^2 + \|L(\sigma - \sigma_{hom})\|^2 \tag{18}$$

where Γ_n^{-1} is used to generate the gaussian noise for voltage measurements V_s, $L_n^T L_n = \Gamma_n^{-1}$, L is the factor from (11) , and σ_{hom} is the best reconstruction from only using the first term as cost function. The inverse is solved using Gauss-Newton optimization with line search and barrier penalty functions for constraints, and we seek to minimize the RMSE:

$$RMSE_E = \sqrt{\frac{1}{N} \sum_{q=1}^{N} (\hat{\sigma}_{true,q} - \hat{\sigma}_{r,q})^2} \tag{19}$$

between $\hat{\sigma}_r$, the final reconstructed conductivity and $\hat{\sigma}_{true}$, the true σ interpolated onto an N-point mesh.

Finally, another important aspect of EIT reconstruction is distinguishability, which characterizes the ability of the model to differentiate between two different internal conductivities σ_1, σ_2 [9]. Rewrite $\sigma_2 = \sigma_1 + \Delta\sigma$, then a metric for distinguishability is the squared norm of boundary voltage differences for a fixed forward method U, which we seek to maximize:

$$\delta_E = \|U(\sigma_1 + \Delta\sigma) - U(\sigma_1)\|^2 \tag{20}$$

4.2 Results and Comparisons

Experiments for the first two metrics (16) (17) are tested on three geometries: a square, a 2×1 rectangle, and a $1 \times 1 \times \sqrt{2}$ right triangle. Coarse and fine mesh element sizes are fixed to be equal to and half of the electrode width, contact impedances $\{z_j\} = 10^{-5} \forall j$, current injections $|i_j| = 1mA$ with $k-1$ injections against electrode 1 (current in at electrode $j, j \neq 1$ and out at electrode 1), and k measurements on adjacent electrode pairs per injection. $N_{\bar{E}} = 2000$ and $N_\sigma = 2000$ were the sample sizes for the neural network, and $N_b = 200$ blob-like conductivities were used to evaluate metrics. Optimized electrode positions are compared against the "standard" uniformly spaced positioning using our metrics. For the square, $\frac{\|\mu_S\|_1}{\|\mu_E\|_1} \approx 18$, indicating that the standard layout had nearly 18 times higher cumulative mean discretization error, μ_S, compared to the optimal μ_E. For the rectangle, $\frac{\|\mu_S\|_1}{\|\mu_E\|_1} \approx 30$, and for the triangle, $\frac{\|\mu_S\|_1}{\|\mu_E\|_1} \approx 1.07$, indicating significantly different reduction effects for different geometries. With regards to conditioning, $\frac{\|\bar{\kappa}_S\|_1}{\|\bar{\kappa}_E\|_1} \approx 3.31$ for the square, $\frac{\|\bar{\kappa}_S\|_1}{\|\bar{\kappa}_E\|_1} \approx 3.62$ for the rectangle, and $\frac{\|\bar{\kappa}_S\|_1}{\|\bar{\kappa}_E\|_1} \approx 1.82$ for the triangle geometry, indicating drastic improvements in conditioning for optimized layouts. Optimized positions for the geometries can be seen in Figure 2.

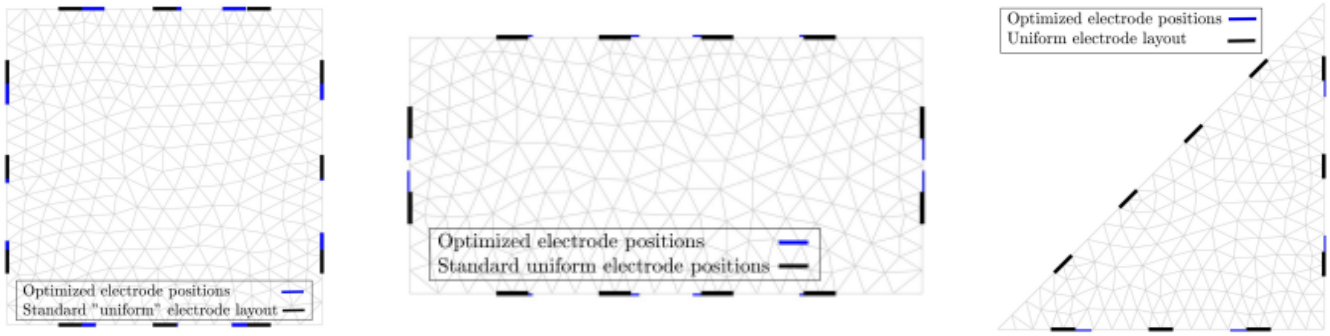

Figure 2: Comparison of optimized (blue) and "standard" electrode layouts (green) on a coarse mesh. $k = 12$ electrodes were fixed for square and rectangle geometries, while $k = 10$ were fixed for the triangle geometry.

Next, experiments for the RMSE metric on inverse reconstruction are conducted by adding gaussian noise η of 1%, 5%, and 10% standard deviation to voltage measurements, and solving for $\hat{\sigma}_r$ in (19) using (18). Conductivities for this part were generated using i) blob-like distributions and ii) ellipsoidal inclusions on a rectangular geometry, with example results in Figure 3, and mesh sizes for forward and inverse solves were fixed (0.04m and 0.075m). Result statistics comparing against a "standard" uniform layout are summarized in Table 1, showing improvements in every case using the optimized layout, albeit less so in ellipsoidal inclusions. Note that this metric is intrinsically biased compared to the previous metrics as it is dependent on simulated data quality.

	Blobby			Ellipsoidal		
	$\eta = 1\%$	$\eta = 5\%$	$\eta = 10\%$	$\eta = 1\%$	$\eta = 5\%$	$\eta = 10\%$
RMSE (%), optimized electrode layout	6.0	7.4	9.8	6.0	8.0	9.7
RMSE (%), "standard" electrode layout	7.6	9.1	14.1	6.0	8.3	11.0

Table 1: Root mean square errors of EIT reconstructions using optimized and uniform electrode layout on "blob-like" and "ellipsoidal inclusion" conductivities. Voltage measurements used in inverse solve were perturbed by Gaussian noise η with 1%, 5%, and 10% standard deviation.

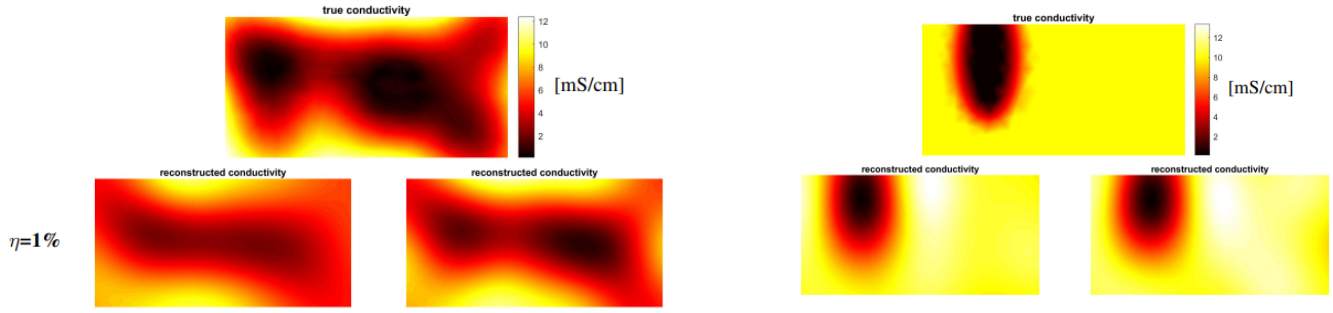

Figure 3: Comparison of recovered conductivities from standard (left reconstructions) and optimized layout electrodes (right reconstructions) for experiments with $\eta = 1\%$ noise added to measured voltages. Left subplot shows comparisons for a blob-like distribution and right subplot shows comparisons for an ellipsoidal inclusion distribution.

Finally, to evaluate our distinguishability metric, 50 blob-like conductivities σ_1 are generated along with 50 blob-like $\Delta\sigma$ on a rectangular geometry, interpolated onto a coarse and a fine mesh. Then, δ_E and δ_S are computed by (20) for optimized and uniform electrode layouts; Figure 4 allows us to observe the improved distinguishability.

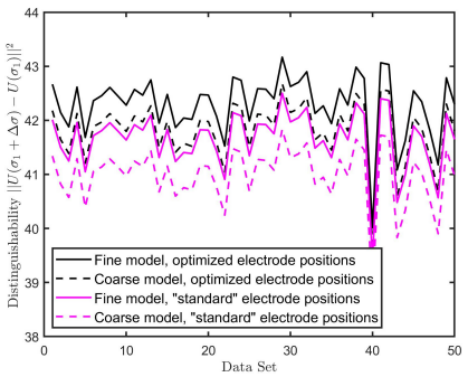

Figure 4: Distinguishability of optimized vs standard electrode layouts on coarse and fine meshes for 50 conductivity samples

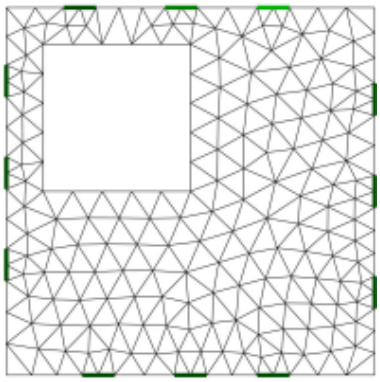

Figure 5: Optimized electrode [positions for square geometry with hole, demonstrating "near-boundary" effects

Lastly, a qualitative effect of optimizing electrodes can be seen in cases of unique geometries–for example, domains with holes. It can be seen in Figure 5 that optimal electrodes tend to cluster near areas with less mesh points (near-boundary effects) to compensate for lack of information. This effect can also be seen in the centralized short side electrodes in Figure 2.

5 Discussion and Future Work

As shown in the results section, optimizing electrode positions using this NN architecture has proven effective in addressing ill-conditioning, discretization, and reconstruction quality problems in EIT compared to the standard electrode layout. However, there remains many avenues of improvement.

First, we can address the prediction method $E = Q_{\bar{\Theta}\bar{E}}([1,0]^T)$, as in practice, $[\kappa,\beta]^T$ will not be close to $[1,0]^T$, as seen by extremely large values of $\kappa = \mathcal{O}(10^{20} - 10^{25})$ in section 4.2. Thus, a different choice of "optimal" Θ may yield a better prediction with respect to the fitting of training data. Additionally, partitioning a larger chunk of the dataset into training (e.g. a 60-20-20 split) may allow for increased learning for more complex geometries and structured conductivity distributions with sharp inclusions [10]–in particular, we may be able to loosen some assumptions on the model as described in section 3. This also ties into the performance of reconstruction metrics on different conductivity distributions, which is another avenue for exploration. As seen in Table 1, currently, optimal layouts improve quality less on sharper, ellipsoidal distributions. An improved ML model that captures

conductivity structure can perhaps develop better performing layouts.

Finally, discretization sensitivity with respect to different geometries can be explored further as well. As seen in section 4.2, the rectangular optimum outperforms the square and triangular ones, with the latter being heavily outperformed in both $\bar{\kappa}_E$ and μ_E metrics. [4] roughly provides intuition on how the forward-calculated voltages of optimized electrodes may be less sensitive to geometries where current is more concentrated towards the center (in contrast, consider electrode deviations from the standard layout in Figure 5), but formalizing justification of this phenomenon has not yet been done to the best of our knowledge and can yield significant insight into the influence of target geometries in EIT.

6 Conclusion

In this project, we have explored an efficient and simple deep learning-based architecture from [4] that effectively optimizes electrode positions in a 2D EIT setting. These optimized electrodes have been shown to outperform standard uniform electrode layouts in various metrics concerning discretization errors, conductivity reconstruction, distinguishability, and ill-conditioning of the Hessian, which directly address the key goals of EIT–to maximize information reliability in measurements and to improve the ill-posedness of the inverse reconstruction problem. Overall, this method is a basic and accessible contribution towards the growing use of deep learning in EIT problems and demonstrates a novel approach that alleviates the requirement of prior conductivity knowledge found in previous works by embedding expected conductivity structures into a neural network.

References

[1] Naqeeb Ali, Joshua Fadelle, and Joshua Zhang. "Electrical Impedance Tomography". SURS Seminar, University of Toronto, Toronto, Canada. Aug. 2025.

[2] Nuutti Hyvönen, Aku Seppänen, and Stratos Staboulis. "Optimizing Electrode Positions in Electrical Impedance Tomography". In: *SIAM Journal on Applied Mathematics* 74.6 (2014), pp. 1831–1851. DOI: 10.1137/140966174. eprint: https://doi.org/10.1137/140966174. URL: https://doi.org/10.1137/140966174.

[3] Christos Dimas et al. "Advances in Electrical Impedance Tomography Inverse Problem Solution Methods: From Traditional Regularization to Deep Learning". In: *IEEE Access* 12 (2024), pp. 47797–47829. DOI: 10.1109/ACCESS.2024.3382939.

[4] Danny Smyl and Dong Liu. "Optimizing Electrode Positions in 2-D Electrical Impedance Tomography Using Deep Learning". In: *IEEE Transactions on Instrumentation and Measurement* 69.9 (2020), pp. 6030–6044. DOI: 10.1109/TIM.2020.2970371.

[5] Andy Adler and William R B Lionheart. "Uses and abuses of EIDORS: an extensible software base for EIT". In: *Physiological Measurement* 27.5 (Apr. 2006), S25. DOI: 10.1088/0967-3334/27/5/S03. URL: https://doi.org/10.1088/0967-3334/27/5/S03.

[6] Liliana Borcea. "Electrical impedance tomography". In: *Inverse Problems* 18.6 (Oct. 2002), R99. DOI: 10.1088/0266-5611/18/6/201. URL: https://doi.org/10.1088/0266-5611/18/6/201.

[7] Guang-Bin Huang. "Huang, G.: Learning Capability and Storage Capacity of Two-Hidden-Layer Feedforward Networks. IEEE Trans. on Neural Networks 14(2), 274-281". In: *IEEE transactions on neural networks / a publication of the IEEE Neural Networks Council* 14 (Feb. 2003), pp. 274–81. DOI: 10.1109/TNN.2003.809401.

[8] Hassan I. Ahmed et al. "A Neural Network-Based Learning Algorithm for Intrusion Detection Systems". In: *Wirel. Pers. Commun.* 97.2 (Nov. 2017), pp. 3097–3112. ISSN: 0929-6212. DOI: 10.1007/s11277-017-4663-8. URL: https://doi.org/10.1007/s11277-017-4663-8.

[9] David Isaacson. "Distinguishability of Conductivities by Electric Current Computed Tomography". In: *IEEE Transactions on Medical Imaging* 5.2 (1986), pp. 91–95. DOI: 10.1109/TMI.1986.4307752.

[10] Yun Xu and Royston Goodacre. "On splitting training and validation set: A comparative study of cross-validation, bootstrap and systematic sampling for estimating the generalization performance of supervised learning". en. In: *J. Anal. Test.* 2.3 (Oct. 2018), pp. 249–262.